A QUASI-ELASTIC LIGHT SCATTERING AND CINEMATOGRAPHIC INVESTIGATION OF MOTILE *CHLAMYDOMONAS REINHARDTII*

T. J. RACEY, R. HALLETT, AND B. NICKEL, *Interdepartmental Biophysics Group, Department of Physics, University of Guelph, Guelph, Ontario, Canada N1G 2W1*

ABSTRACT Quasi-elastic light scattering and cinematographical techniques were used to investigate the motility of *Chlamydomonas reinhardtii* (wild type). It was found that quantitative information on the trajectory of motion was required for a meaningful interpretation of the autocorrelation functions. Two models for describing the oscillatory motion of the cell were developed; one based on the instantaneous forward-and-backward motion of the cell, and the other based on a sinusoidal perturbation to the average forward motion. Both models gave satisfactory agreement with the shape of the experimentally measured autocorrelation function, thus making it possible to use this measurement to determine mean progressive swimming velocities in a population of >200 cells.

INTRODUCTION

A computational investigation of motile ellipsoids by Craig et al. (1979) suggested that the experimental electric field autocorrelation functions of light scattered from large motile cells should fall into three categories: (*a*) functions whose decay times are inversely related to the rotational motion of the cell, (*b*) functions whose decay times are inversely related to the translational speed of the cell, and (*c*) functions whose decay time depends on both the rotational motion and translational speed of the cell. Their studies indicated that normal bull spermatozoa yielded functions of category (*a*).

In this paper motile *Chlamydomonas reinhardtii* cells are shown to yield functions of category (*b*). This conclusion is based on a comparison of experimentally determined functions obtained over a range of scattering angles with functions calculated on the assumption that the cells behave as translating Rayleigh-Gans-Debye (R-G-D) particles. The swimming parameters obtained from the light-scattering experiments were consistent with those obtained from high-speed cinematography.

THEORY

The following discussion treats the cells as an ellipsoidal R-G-D particle of semiaxes *a*, *b*, and *c*. The general case of a particle moving about an axis that may or may not coincide with an axis through its center of mass has been given by Holz and Chen (1978). The theory was extended by Craig et al. (1979) to cover the analysis of bull sperm. The treatment here follows the discussion of Craig et al. (1979).

The electric field autocorrelation function, $g^{(1)}(\tau)$, can be written as

$$g^{(1)}(\tau) = C_n^{-1} \langle e^{i\vec{k}\cdot[\vec{r}(\tau)-\vec{r}(0)]}\, e^{i\vec{k}\cdot[\vec{R}(\tau)-\vec{R}(0)]}\, A(\vec{k}, \tau)\, A^*(\vec{k}, 0) \rangle, \tag{1}$$

where C_n is a normalization factor, τ is a delay time, $\vec{r}(t)$ and $\vec{R}(t)$ are the components of the instantaneous position of the scatterer along and perpendicular to the axes of motion, respectively. $A(\vec{k}, \tau)$ is the form factor for the ellipsoidal particle, which can be shown to be

$$A(\vec{k}, \tau) = 3 j_1(K)/K \tag{2}$$

where j_1 is the spherical Bessel function of order 1. The brackets $\langle\ \rangle$ in Eq. 1 indicate additional averaging over characteristics of the motion, such as the progressive swimming speed v.

Computation of Eq. 1 can be simplified by expressing the periodic terms (Craig et al., 1979) as a Fourier expansion. This yields, for the case having $R(\tau) = 0$:

$$g^{(1)}(\tau) = C_n^{-1} R \int_{-1}^{1} d\nu\, e^{ik\nu v\tau} \sum |B_n|^2 e^{in\omega\tau}, \tag{3}$$

where $\nu = \cos\theta$, the Fourier coefficients B_n depend on the shape and trajectory of the cell, and R signifies the real part only. If the rotational motion of the cell is small ($\omega \approx 0$), the averaging process in Eq. 3 simplifies to the form (Nossal, 1971)

$$\langle e^{ik\nu v\tau} \rangle = \int_0^\infty e^{ik\nu v\tau} P_s(v)\, dv, \tag{4}$$

where $P_s(v)$ is the swimming speed distribution function of the motile cells. With this simplification Eq. 3 reduces to:

$$g^{(1)}(\tau) = \int_0^\infty dv \int_{-1}^{1} d\nu\, P_s(v)\, e^{ik\nu v\tau} \sum_n |B_n|^2. \tag{5}$$

Eqs. 3–5 assume that the translational motion of the particle is linear for times greater than $(kv)^{-1}$. In these experiments the minimum value of k is $\sim 3.5\ \mu m^{-1}$, and the average progressive speed of the cells was determined cinematographically to be $\sim 84\ \mu m\ s^{-1}$. Since the cells swim in straight lines for a second or longer, this assumption appears to be justified.

Our strategy in this study was to develop a suitable expression for $P_s(v)$ for *C. reinhardtii* from high-speed cinematographic analysis. The function $P_s(v)$ thus determined was used in conjunction with Eq. 5 to calculate electric field autocorrelation functions over a range of accessible scattering angles. These expected autocorrelation functions are compared with experimental ones in the results section.

EXPERIMENTAL PROCEDURES

The *C. reinhardtii* (wild type: ATCC 18798) culture was acquired from the American Type Cell Culture Collection, Rockville, Md. The culture was grown in medium 277 as described by the ATCC, without the agar and with a chemically equivalent weight substitution of $(Na)_2MoO_4 \cdot 2H_2O$ for the $(NH_4)_2MoO_4$. The medium had a pH (adjusted) of 6.8. The cells were kept at 25°C, under a broad spectrum Grolux light (Sylvania, Montréal), with 15 h of light and 9 h of darkness daily.

To prepare the sample, the test tube containing a *C. reinhardtii* culture, which had been started anywhere from 4 to 13 d previously, was removed from the incubator 1 h into its light cycle. It was spun

down in a centrifuge at ~1,000 rpm for 5 min, and the supernate was removed and replaced by fresh medium; the pellet was then completely resuspended by gentle agitation, and the sample was returned to the incubator. This ensured that all cells had potential access to the fresh nutrient, so as to maximize active behavior. The cells were incubated in this medium for 60–90 min, after which the suspension was respun in a centrifuge at 1,000 rpm for 5 min. The sample was then replaced in the incubator for another 90 min, which allowed time for the motile swimmers to swim up several centimeters into the medium. The cells were always ~4 h into their light cycle before experiments were begun. This was done to minimize changes induced by light. It was noted that the activity of the cells decreased considerably after the cell had been in the light for 12 or more h. The incubation, microscope stage, and light scattering chamber temperatures were kept at ~24.8 ± 0.3°C throughout these studies.

Cinematography

The samples used in the cinematography were prepared as described above. A few drops of the upper layer of the sample were placed in a round well microscope slide which was then covered by a slip cover. The sample was then examined under a light microscope (KL14, Carl Zeiss, Inc., New York). A wall-mounted Locam high-speed motion picture camera (model 51, Redlake Corporation, Campbell, Calif.), capable of speeds up to 500 frames/s, was aligned with the barrel of the microscope, so that the camera floated about the barrel but did not touch it. This ensured that any vibrations from the camera would not be transmitted to the microscope and then to the motile cells. The cells in the cylindrical well were photographed using 16 mm Kodak 4X-reversible film (ASA 400, Eastman Kodak Co., Rochester, N.Y.) at various film speeds and under different magnifications. A reticle was used under each magnification to allow a distance calibration to be determined.

The film was analyzed using an L-W International photo optical data analyser (model 224, Woodland Hills, California), which is capable of going from still frame to still frame, or up to 24 frames/s. The image on the frame was magnified by reflecting the image off a 45° mirror onto a glass table. The projector-mirror-table distance was fixed for all analysis so that intercomparison of film would be possible. The exact frame rate was determined from the 0.01-s timing marks on the film that were projected on to the table. The motion of the cells and their dimensions were then analyzed by the measurement of their images on this table.

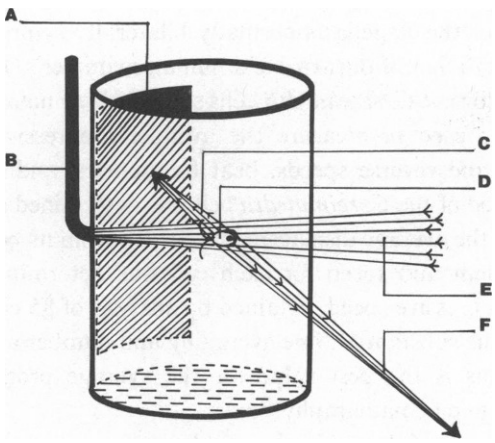

FIGURE 1 Diagram of the scattering cell showing large scattering angle arrangement. The cell is mounted inside a cylindrical brass block. *A*, movable black absorbing shield to eliminate all reflection of forward scatter; *B*, black tube to absorb main beam; *C*, forward scatter from particle; *D*, *Chlamydomonas* cell (scatterer); *E*, light cone from laser; *F*, backward scatter to detector.

Light Scattering

The samples for the light scattering experiments were withdrawn from the supernate, counted by hemocytometry, and diluted so as to obtain a final concentration of $0.8 \rightarrow 1.5 \times 10^6$ cells/ml. This concentration insured that the number of cells within the scattering volume was sufficiently large (>200) to preclude effects due to number fluctuations.

Two scattering chambers were used in these experiments. The first, employing a square cell, was used for scattering angles of between 15° and 30°. The second, employing a round scattering cell, allowed scattering angles from 20° to 150° to be monitored. The design of this round cell was important because large biological cells tend to scatter much more strongly in the forward than in the backward directions. Extreme care must always be taken to remove the main beam completely after one pass through the scattering volume. This scattering chamber uses a black tube which has fluid continuity with the interior of the chamber as a beam stop (Fig. 1). When fluid is drawn up the tube, all reflecting interfaces are eliminated. Second, a black shield must be placed on the inside wall of scattering chamber opposite to the detector. This prevents low-angle scattered light from reflecting and overpowering the backscattered signal. Both these refinements are a necessity for scattering vector-dependence studies. A calibration experiment done using 1.0-μm latex spheres yielded consistent results at all angles from 20° to 150°. Temperature control in the scattering chamber was effected by a feed-back regulation of heating elements integrated into the top of the brass block housing the scattering chamber. Thus, all samples were heated top down, which eliminated thermal convection currents. Sample temperatures were monitored by a calibrated thermal transistor (Analog Devices, Inc., Norwood, Mass.) located 0.5 cm from the scattering volume.

EXPERIMENTAL RESULTS

Cinematography

The swimming motion of *C. reinhardtii* has been described by Ringo (1967) and Hyams and Borisy (1978). The cells normally travel with the flagella-bearing end toward the direction of motion. At the beginning of the effective stroke the flagella are straight and extended forward. The flagellum sweeps backward, remaining fairly straight and bending near the base. The recovery stroke begins as the effective stroke is completed, with a wave of bending passing along the flagellum from base to tip. This restores the flagellum to its original position. The positional relationship of the flagella is normally bilaterally symmetrical, the synchrony of motion being analogous to that of the arms of a human swimmer's breast stroke. Both flagella beat in the same plane so that *C. reinhardtii* cells show little or no rotation as they swim.

Cinematography was used to measure the average progressive speeds, as well as the instantaneous forward and reverse speeds, beat frequencies, and sizes of several cells. An average progressive speed of the *C. reinhardtii* cell was determined at low frame rates (30–50 frames/s) by recording the average displacement of a cell from its position five frames earlier. The average displacement and speed for each cell was determined from a total of ~200 frames. The average progressive speed, obtained by analysis of 85 cell tracks, was found to be 84 μm s^{-1}. Because of the substantial time averaging and number averaging involved, we feel that for our sample this is the best value for the average progressive speed of the cell population available from cinematography.

The distribution of speeds of these 85 cells was determined, and the results are shown in the histogram in Fig. 2. This distribution could be modeled with the equation:

$$P_s(v) = \frac{128}{3\bar{v}^4} v^3 e^{-4v/\bar{v}}. \quad (6)$$

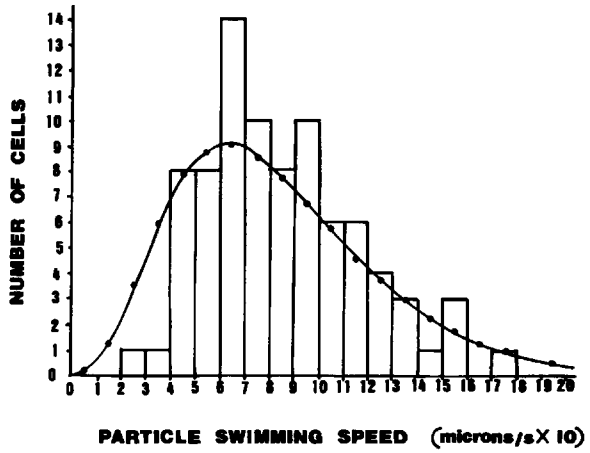

FIGURE 2 Speed distribution histogram of the *C. reinhardti* cells. The superimposed function is $P_s(v) = (128/3\bar{v}^4)\, v^3\, e^{-4v/\bar{v}}$ normalization factor = number of cells (85) × interval (10 μm s^{-1}).

This function, properly normalized, is shown superimposed on the histogram in Fig. 2. The value of $\bar{v}$ used here was 84 μm/s, the mean of the cell speeds.

The instantaneous motion of the *C. reinhardtii* cells was examined by using higher frame rates (100–200 frames/s) and frame-by-frame analysis. A cell track was selected for measurement if it appeared to be moving in a straight line without contacting other cells. An arbitrary origin was picked and the displacement of the cell from this origin as a function of frame number was recorded. This analysis was performed for 12 cells. In each case results were similar to those shown in Fig. 3. The average progressive speeds of these 12 cells were determined from the average slope of these graphs. The results are tabulated in Table I. A relative ratio of cell movement for forward, backward, or stationary motion for successive frames was determined from the data of the graphs such as Fig. 3. This gave a fraction for forward moving motion of $N_f = 0.57 \pm 0.06$, reverse moving motion of $N_b = 0.32 \pm 0.06$, and a stationary fraction of about $N_s = 0.11 \pm 0.06$.

The oscillating curves, such as in Fig. 3, appear similar to a sine wave superimposed on a ramp function. The amplitudes of these curves were measured, and are also shown in Table I.

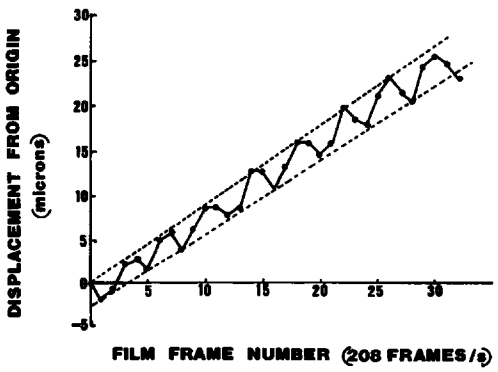

FIGURE 3 Characteristic motion of a *C. reinhardtii* cell.

TABLE I
CINEMATOGRAPHIC DATA FOR 12 CELLS

Cell number	Average forward speed	Average reverse speed	Amplitude of oscillation about mean	Average progressive speed	Frequency of local displacement from mean path
	(μm/s)	*(μm/s)*	*(μm)*	*(μm/s)*	*(Hz)*
1	198 ± 66	100 ± 57	1.16	57	24 ± 3
2	252 ± 51	124 ± 69	1.65	96	26 ± 3
3	311 ± 114	148 ± 40	1.32	142	44 ± 9
4	311 ± 66	228 ± 71	1.16	120	66 ± 23
5	526 ± 201	301 ± 52	2.15	154	59 ± 22
6	377 ± 110	260 ± 90	1.40	135	53 ± 8
7	488 ± 80	293 ± 86	1.49	177	56 ± 7
8	410 ± 178	252 ± 121	1.82	111	47 ± 6
9	469 ± 147	220 ± 63	1.62	157	49 ± 5
10	522 ± 154	276 ± 98	1.65	121	54
11	296 ± 141	200 ± 72	1.32	114	55
12	389 ± 219	213 ± 56	1.65	103	50
Average value of each column	$\bar{v}_f = 379 \pm 108$	$\bar{v}_b = 218 \pm 65$	$\bar{A} = 1.53 \pm 0.29$	$\bar{v} = 124 \pm 32$	$\bar{f} = 49 = 12$

The general pattern of motion demonstrated in Fig. 3 is rather interesting. The Reynolds number, R_e, of a *C. reinhardtii* cell can be estimated from:

$$R_e = \frac{\bar{v}\, L}{\nu}, \tag{7}$$

where ν is the kinematic viscosity (10^{-2} cm^2 s^{-1} for water), $\bar{v}$ is the average progressive speed, and L is the diameter of the cell. An average speed $\bar{v} = 84$ μm s^{-1} and size $L = 10$ μm yield a value for R_e of $\sim 10^{-3}$, which means that the swimming cell is well within the Stokesian realm. Thus, the momentum of the cell is almost instantly diffused throughout the field: the cell is unable to glide and its motion is tightly coupled to the movement of the flagella. One would, therefore, expect the cell to move in reverse during the recovery stroke of the flagella, an effect obvious in Fig. 3.

Values for the speeds of the cell going forward and going backward were determined from the positive and negative slopes within the oscillators. Results for the data in Fig. 3 are given in Table II. The average forward speed for $\bar{v}_f = 488 \pm 80$ μm/s and the average reverse speed for $\bar{v}_b = 293 \pm 86$ μm/s. Averages for all twelve cells are listed in Table I.

A reticle was employed to calibrate the displacements observed cinematographically. Dimensions of the *C. reinhardtii* cells were also measured from the film. Most cells appeared to be slightly ellipsoidal. The results in Table III show values of the long diameter (c), and the shorter diameters (a and b), as averaged from a total of 68 cells.

Light Scattering

Electric field autocorrelation functions [$g^{(1)}(\tau)$] were obtained over scattering angles from 15° to 150° with a minimum of five separate experiments performed at each angle. The functions

TABLE II
FORWARD AND REVERSE VELOCITIES OF THE CELL SHOWN IN FIG. 3

Forward velocity	Reverse velocity
(μm/s)	
$v_1 = 320$	$v_1 = 411$
$v_2 = 446$	$v_2 = 275$
$v_3 = 480$	$v_3 = 343$
$v_4 = 480$	$v_4 = 137$
$v_5 = 549$	$v_5 = 411$
$v_6 = 549$	$v_6 = 275$
$v_7 = 549$	$v_7 = 240$
$v_8 = 549$	$v_8 = 275$
	$v_9 = 275$
$\bar{v}_f = 488 \pm 80$	$\bar{v}_b = 293 \pm 86$

Cell freq, 56 ± 7 Hz; average speed, 177 μm/s; amplitude of oscillation about mean path, 1.49 μm.

exhibited the classic shoulder, which signifies the presence of motile particles (Figs. 4 and 5).

The order in which the various scattering angles were chosen was scrambled for any one sample so that no systematic aging effect would be observed. The autocorrelation functions were plotted out as the experiment proceeded, to ensure a consistent decay time for each function. The results of all the samples recorded at each angle were averaged to give a single half-width time (HWT) value for each scattering angle. The results are shown in Table IV. The 20° scattering angle was used as the primary scattering angle, since it could be measured with either of the two scattering cells; this is why so many measurements are shown at this particular angle. These results were plotted in Fig. 6, scaled against $1/\sin(\theta/2)$, where θ is the scattering angle.

MODELING THE CORRELATION FUNCTION

Any physically meaningful model for the interpretation of the scattering functions must have the characteristics of the cells and their motion as a foundation. In the following sections we

TABLE III
DIMENSIONS OF *C. REINHARDTII* CELLS

Magnification (objective)	c	a, b	Number of cells
	(μm)		
× 100	7.7 ± 1.3	6.6 ± 1.3	18
× 40	12.4 ± 1.1	10.2 ± 0.9	12
× 40	12.3 ± 1.2	10.0 ± 1.2	12
× 40	14.5 ± 2.6	12.1 ± 2.1	15
× 40	9.2 ± 1.1	6.9 ± 1.3	11

Diameters: $\bar{c}$, 11.2 ± 2.7 μm; $\bar{a}$, $\bar{b}$, 9.2 ± 2.4 μm.

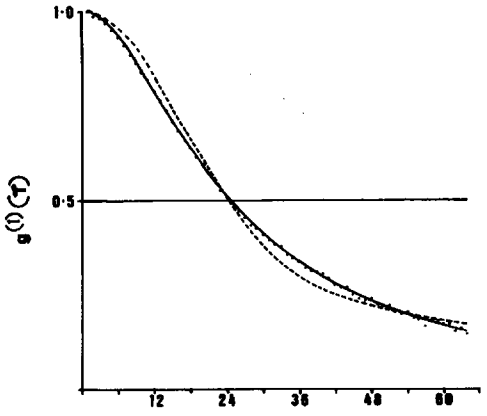

FIGURE 4

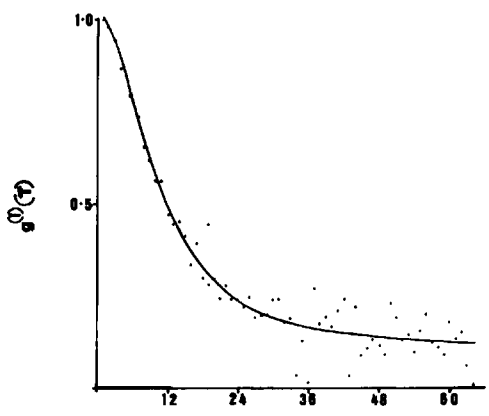

FIGURE 5

FIGURE 4 An autocorrelation function at $\theta = 15°$. A least-squares fit to the points (solid line) using Eqs. 5, 8, and 9 to yield fit parameters $X_2 = 0.40$, $\bar{v}_2 = 336$ μm/s, $X_1 = 0.50$, $\bar{v}_1 = 136$ μm/s, $X_0 = 0.10$ with a standard deviation = 1.44×10^{-3}. The parameters are comparable to Eq. 10. The bin time per channel is 120 μs. The dashed line is the sine function model of Eq. 14 with $\bar{v} = 84$ μm s^{-1}, $f = 34$ Hz, and $A = 1.29$ μm.

FIGURE 5 An autocorrelation at $\theta = 110°$. A least-squares fit to the points (solid lines), as before, yields fit parameters $X_2 = 0.32$, $\bar{v}_2 = 352$ μm/s, $X_1 = 0.47$, $\bar{v}_1 = 168$ μm/s, $X_0 = 0.21$ with a standard deviation = 1.5×10^{-1}. The parameters are comparable to Eq. 10. The bin time per channel is 40 μs.

TABLE IV

THE HWT OF THE EXPERIMENTAL ELECTRIC FIELD AUTOCORRELATION FUNCTION AS A FUNCTION OF SCATTERING ANGLE

Scattering angle	Number of samples	Average half-width time of electric field autocorrelation function	$\frac{1}{\sin\left(\frac{\theta}{2}\right)}$
(°)		(ms)	
15	7	2.92 ± 0.20	7.66
20	12	2.17 ± 0.19	5.76
25	6	1.76 ± 0.26	4.62
30	7	1.48 ± 0.11	3.86
40	5	1.11 ± 0.07	2.92
50	5	0.92 ± 0.06	2.37
60	6	0.73 ± 0.07	2.00
70	6	0.65 ± 0.01	1.74
80	5	0.55 ± 0.07	1.56
90	5	0.50 ± 0.05	1.41
100	5	0.46 ± 0.04	1.31
110	5	0.44 ± 0.03	1.22
120	5	0.40 ± 0.03	1.15
130	4	0.40 ± 0.04	1.10
140	5	0.47 ± 0.04	1.06
150	5	0.60 ± 0.07	1.04

provide two alternate methods for interpreting the experimental functions. The strengths and weaknesses of each method will be demonstrated.

Two-Speed Distribution Model with a Stationary Function

The high-speed cinematography had indicated that the *C. reinhardtii* cell, although having a net movement along a straight path, could be found either moving forward or backwards along that path, for times long compared with $(kv)^{-1}$. The average speeds for the forward-and-reverse motion were different, which suggests that the swimming speed distribution, $P_s(v)$, could be composed of two distributions, each with its own average velocity. This would give a distribution for $P_s(v)$ similar to Eq. 6 but with high speed (v_2) and slow speed (v_1) terms

$$P_s(v) = X_2 \frac{128}{3\bar{v}_2^4} v_2^3 e^{-(4v_2/\bar{v}_2)} + X_1 \frac{128}{3\bar{v}_1^4} v_1^3 e^{-(4v_1/\bar{v}_1)}, \tag{8}$$

where X_2 is the fraction of particles moving relatively quickly, and X_1 is the fraction of particles moving relatively slowly. The shape of the curve in Fig. 3 indicates that at some times the cell shows no motion in successive frames. The scattering function of these stationary cells was described by a function which was obtained from a polynomial fit of the experimental autocorrelation function of dead cells. It is given by

$$\text{Stationary} = [1 - (X_2 + X_1)][1 - k^2t(-0.30209 + k^2t\{-0.27928 [0.45634 - k^2t(0.33518)]\})], \tag{9}$$

where t is the delay time. Thus function provides the "background" for the motile cell function.

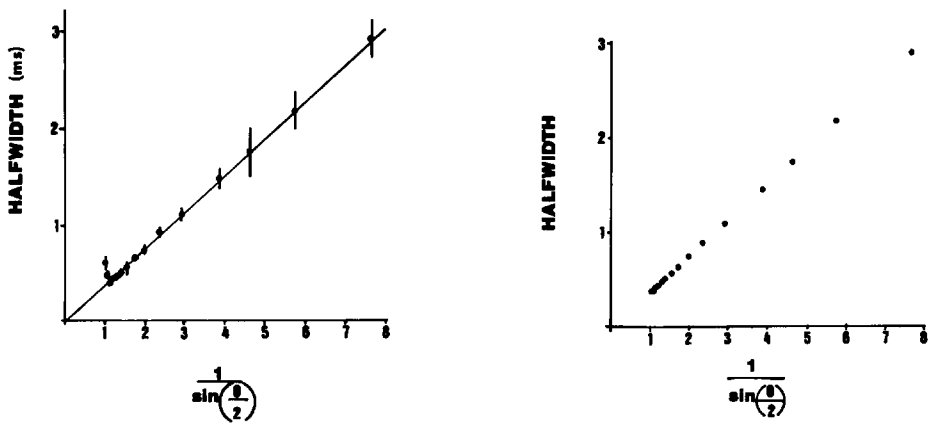

FIGURE 6 The HWT (ms) of the experimental electric field autocorrelation function scaled against 1/sin ($\theta/2$), where θ = scattering angle. The solid line represents a least-squares fit to all except the first two points.

FIGURE 7 This plot represents the scaling curve (HWT vs. 1/sin ($\theta/2$) of both models. The two speed distribution model with a stationary function has the parameters $X_2 = 0.35$, $\bar{v}_2 = 357$ μm s^{-1}, $X_1 = 0.49$, $\bar{v}_1 = 161$ μm s^{-1}, $X_0 = 0.16$. The sine function model has the parameters $\bar{v} = 84$ μm s^{-1}, $f = 34$ Hz, $A = 1.29$ μm.

TABLE V
THE HWT OF THE ELECTRIC FIELD AUTOCORRELATION FUNCTION DETRMINED FROM THE TWO-SPEED DISTRIBUTION MODEL WITH A STATIONARY FUNCTION

Angle	HWT
(°)	(ms)
15	2.92
20	2.19
25	1.75
30	1.46
40	1.11
50	0.89
60	0.75
70	0.64
80	0.57
90	0.51
100	0.47
110	0.44
120	0.41
130	0.39
140	0.38
150	0.37

$X_2 = 0.35$, $X_1 = 0.49$, $N_0 = 0.16$, $\bar{v}_2 = 357.0\ \mu m\ s^{-1}$, $\bar{v}_1 = 161.0\ \mu m\ s^{-1}$, $\bar{v}_0 = 0\ \mu m\ s^{-1}$.

Eq. 5 was simplified by making the assumption, based on the shape of the scaling curve of the experimental electric field autocorrelation function HWT as a function of $1/k$, that the cells were scattering as if they were spheres. Computational studies (Hallett et al., unpublished data) have indicated that the oscillations in this scaling curve are due solely to the form factor of the cell, and that linear scaling curves of this type arise from spherical particles. Eqs. 8 and 9 were then substituted into the new simplified Eq. 5.

The four parameters in Eqs. 5, 8, and 9 were then obtained by least-squares fit to the experimental autocorrelation functions. The average values of the four parameters were found over all accessible scattering angles to be:

$$X_2 = 0.36 \pm 0.05 \qquad \bar{v}_2 = 357 \pm 25\ \mu m/s$$
$$X_1 = 0.49 \pm 0.02 \qquad \bar{v}_2 = 161 \pm 23\ \mu m/s$$
$$X_0 = 0.15 \pm 0.07 \tag{10}$$

Examples of the goodness of the fit to individual autocorrelation functions are shown in Figs. 4 and 5. The parameters in Eq. 10 were used in Eq. 5 to calculate a scaling curve. The results of this scaling curve are shown in Table V and graphed in Fig. 7.

The results of Eq. 10 can be compared with cinematographic data from 12 cells (Table I). The corresponding parameters from the cinematography were:

$$N_f = 0.57 \pm 0.06 \qquad \bar{v}_f = 379 \pm 108\ \mu m/s \tag{11}$$

and

$$N_b = 0.32 \pm 0.06 \qquad \bar{v}_b = 218 \pm 65\ \mu m/s$$
$$N_s = 0.11 \pm 0.06 \tag{12}$$

The differences in the values X_2 and N_f (and X_1 and N_b) arise because light scattering measures speeds and not velocities. This point will be described more fully in the discussion.

Sine Function Model

The curve of the cellular motion shown in Fig. 3 has similarities to a sine function superimposed on a ramp function such that

$$r(\tau) - r(0) = \bar{v}\,\tau + A[\sin(\omega t + \phi) - \sin\phi], \tag{13}$$

where $\bar{v}$ is the slope of the ramp (i.e., the average velocity), A is the amplitude of the oscillation, ω is the angular frequency of the oscillation, and ϕ is the phase of the starting point. This equation was substituted into Eq. 1 for $[\vec{r}(\tau) - \vec{r}(0)]$, again on the assumption of a spherical shape and the speed distribution of Eq. 6. This yields

$$g^{(1)}(\tau) = \int_{-1}^{1} d\cos\theta \frac{\left[\left(\frac{4}{\bar{v}}\right)^4 + kt\cos\theta)^4 - 6\left(\frac{4}{\bar{v}}\right)^2 (kt\cos\theta)^2\right]}{\left[\left(\frac{4}{\bar{v}}\right)^2 + (kt\cos\theta)^2\right]^4} J_0\left[2\cos\theta\, kA \sin\left(\frac{\omega t}{2}\right)\right], \tag{14}$$

where J_0 is the zero order Bessel function and θ is the angle between $\vec{k}$ and $\vec{r}(\tau)$. Eq. 14 was

TABLE VI
THE HWT OF THE ELECTRIC FIELD AUTOCORRELATION FUNCTION DETERMINED FROM THE MODEL: $r(\tau) = \bar{v}t + A[\sin(\omega t + \phi) - \sin\phi]$

Angle	HWT
(°)	(ms)
15	2.92
20	2.18
25	1.75
30	1.46
40	1.10
50	0.89
60	0.75
70	0.66
80	0.59
90	0.53
100	0.49
110	0.46
120	0.44
130	0.42
140	0.40
150	0.39

The values of the parameters used in the determination were: $\bar{v} = 84\ \mu m/s$, $\nu = 34$ Hz, and $A = 1.29\ \mu m$.

solved numerically for different values of the parameters. This was not done with a least-square program since Eq. 14 is not analytical. In order to obtain a scaling curve similar to Fig. 6, the value of $\bar{v}$ was assumed to be equal to the average of the speed distribution, 84 μm/s, and the value of ω was determined from the average frequency of the 12 cells in Table I scaled by the factor (84/128). This was justified by cinematographic observation that a linear relationship occurred between the frequency of oscillation and the average velocity of the cell. This scaling gave a value for the average flagellar frequency of ~34 Hz. The values of A were modified until a HWT similar to the experimental values was found. The results are shown in Table VI and Fig. 7. The results of the parameters obtained, namely $\bar{v} = 84$ μm/s, $f = 34$ Hz, and $A = 1.29$ μm, were used to compute individual autocorrelation functions. This value of A compares well with the cinematographic value of 1.53 ± 0.29 μm from the 12 cells. The result of this autocorrelation function obtained with the model was superimposed on Fig. 4.

DISCUSSION

The Two-Speed Distribution with a Stationary Function

The two-speed distribution model with the swimming speed distribution function of Fig. 2 gives a scaling curve for the *C. reinhardtii* cells that is very similar to that obtained experimentally. The least-square fit to the individual correlation functions gives four parameters which are consistent over the whole of the scaling curve.

The average value of the average progressive speed can be obtained from the cinematographic data in Table I. For the 12 cells:

$$\bar{v}_{12} = N_f \bar{v}_f - N_b \bar{v}_b,$$

$$\bar{v}_{12} = 0.58 \times 379 - 0.32 \times 218,$$

$$\bar{v}_{12} = 146\ \mu\text{m s}^{-1}. \tag{15}$$

This compares with the measured average progressive speed, from the average slopes, of $\bar{v} = 124 \pm 32$ μm/s for these same cells.

The value of the average progressive speed of the cells can be determined from the light-scattering data once the four fit parameters (X_2, $\bar{v}_2$, X_1, $\bar{v}_1$) are related to the four parameters of Eq. 15. When the least-square program is fitting Eq. 8 to experimental autocorrelation functions, it is actually trying to replace the cellular motion, such as in Fig. 3, with a series of three line segments which are characterised by their slopes: $\bar{v}_2 = 357$ μm/s, $\bar{v}_1 = 161$ μm/s, and $\bar{v}_0 = 0$ μm/s. It determines the relative ratios of these line segments to give the best possible fit. The best-fit speeds are similar to the physical forward-and-backward motion of the cells as determined by cinematography, $\bar{v}_f = 379 \pm 108$ μm/s, $\bar{v}_2 = 357 \pm 25$ μm/s, $\bar{v}_b = 218 \pm 65$ μm/s, and $\bar{v}_1 = 161 \pm 23$ μm/s.

This agreement suggests that we can associate $\bar{v}_2$ with the forward fast motion of the cell, and $\bar{v}_1$ with the slower, reverse motion of the cell. But the corresponding fractions found, namely $N_f = 0.57$ ($X_2 = 0.36$) and $N_b = 0.32$ ($X_1 = 0.49$) differ considerably.

This problem arises because the least-squares fit program uses some of the slopes more than once. It appears that the program uses X_2 for the forward motion plus part of X_1, with the remainder of X_1 being associated with the reverse motion. Schematically, this configuration is shown in Fig. 8. The segments *a* and *b* are both forward motions, *a* being associated with $\bar{v}_2$

and b with $\bar{v}_1$. The reverse motion is then represented by c, associated with the slower motion. Both b and c would have the same magnitude for their slope, namely $\bar{v}_1 = 161$ μm/s. Segment d would be the stationary function. Following the scheme of Fig. 8, we can write:

$$N_f = X_{1f} + X_2$$
$$N_b = X_1 - X_{1f}, \tag{16}$$

where X_{1f} is the component of X_1 that corresponds to segment b. The parameters in Eq. 16 are constrained by Eqs. 10–12. Using the speeds of Eq. 10, we should be able to derive a series of parameters to describe the average progressive speed of the 12 cells described in Table I. The description in Fig. 8 together with Eq. 15 gives

$$\bar{v} = X_2 \bar{v}_2 + X_{1f} \bar{v}_1 - (X_1 - X_{1f}) \bar{v}_1, \tag{17}$$

where $X_2 = 0.36$. This yields $X_{1f} = 0.21$ and an average progressive speed

$$\bar{v} = 0.36 \times 357\ \mu\text{m s}^{-1} + 0.21 \times 161\ \mu\text{m s}^{-1} - (0.49 - 0.21) \times 161\ \mu\text{m s}^{-1},$$
$$\bar{v} = 117\ \mu\text{m s}^{-1}. \tag{18}$$

This value compares well with the $\bar{v}$ determined for data in Table I of 124 ± 32 μm s^{-1}, and therefore the result for $\bar{v}$ appears to be consistent with the model of Eq. 16 and Fig. 8.

One problem then is to find values of X_{1f} that relate to the "average" *C. reinhardtii* cell, and not just to the 12 cells of Table I. A set of parameters that could be used to describe the average cell, and still adhere to the constraints found in the least squares fit of Eq. 10 is obtained if one chooses $X_{1f} = 0.11$. This gives

$$\bar{v} = 0.36 \times 357\ \mu\text{m s}^{-1} + 0.11 \times 161\ \mu\text{m s}^{-1} - (0.49 - 0.11) \times 161\ \mu\text{m s}^{-1},$$
$$\bar{v} = 85\ \mu\text{m s}^{-1}, \tag{19}$$

and number fractions of $N_f = 0.47$, $N_b = 0.38$, and $N_s = 0.15$ for the average cell. A comparison of the results of the parameters in Eq. 19 with those of Eqs. 11 and 12 seems to indicate that what makes a cell a faster swimmer is the fraction N_f, since the other fractions N_b and N_s agree within the deviation for both the 12 cells ($\bar{v} = 124$ μm s^{-1}) and the average cell ($\bar{v} = 84$ μm s^{-1}).

This model seems particularly good for fitting individual experimental results, but is

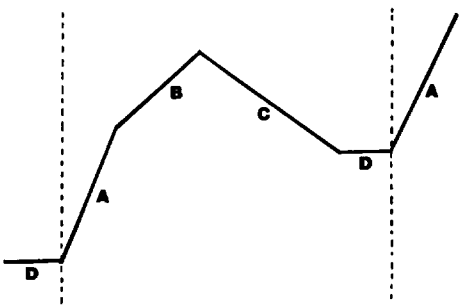

FIGURE 8 Schematic diagram of the segments used in the two-speed distribution model with a stationary function least-squares fit. $A = \bar{v}_2$, $B = \bar{v}_1$, $C = \bar{v}_1$, $D = \bar{v}_0 = 0$ μm s.

slightly weak in uniquely determining an expression for the average cell. Thus, with this approach the light scattering data can be interpreted only after a "calibration" has been done with the aid of cinematographic information.

Sine Function Model

The sine function model with the swimming speed distribution model of Fig. 3 gives a scaling curve for the *C. reinhardtii* cells that is also very similar to that obtained experimentally. The computed scaling curve requires values for $\bar{v}$, ω, and A that are similar to the values of the parameters obtained cinematographically (Table I).

The problem with this model is quite apparent in Fig. 4. The model provides a shoulder that is too large for the data and tends to oscillate about the experimental function. In our opinion the fit is not unreasonable, but it is just not as good as the two-speed distribution function model. It was thought that different sets of parameters that gave the same HWT might fit the correlation function better. In each of these cases the fit to the experimental correlation was no better, and in fact probably worse, since in each case the shoulders were the same, but the tail leveled off flatter (from about channel 36 out). It appears that the parameters $\bar{v}$ = 84 μm/s, A = 1.29 μm, and f = 34 Hz were the best parameters available.

It appears that the sine function model does a good job of modeling the average cell, in that all of the model parameters are in agreement with cinematographical results, but this model is only fair in fitting a particular experimental autocorrelation function. It is possible that extending the sine function to higher order terms might improve the fit.

The results of the parameters obtained in the work done here can be compared with the parameters quoted in the literature (see Table VII).

It was noted in Fig. 6 that the values of HWT for scattering angles of 140 and 150° do not fall in the same apparent linear relationship displayed by the values of HWT for the other

TABLE VII
A BRIEF COMPARISON BETWEEN THE PARAMETERS OBTAINED IN THIS INVESTIGATION AND THE LITERATURE

Reference	Average progressive speed: $\bar{v}$
Racey, Hallett, and Nickel	
Cinematography: long time average, 85 cells	84 μm/s
Cinematography: detailed study, 12 cells	124 ± 32 μm/s
Two-speed model for average cells	
N_f = 0.47, N_b = 0.38, N_s = 0.15	85 μm/s
Two-speed model for 12 cells	
N_f = 0.57, N_b = 0.32, N_s = 0.11	117 μm/s
Sine function model for average cell	
$\bar{v}$ = 34 Hz, A = 1.29 μm	84 μm/s
Nakamura, S. (1979)	≃100 μm/s
Bean and Harris (1979)	≃75 μm/s
	Beat frequency: $\bar{\nu}$
Racey, Hallett, and Nickel	≃34 Hz
Nakamura, S. (1979)	≃30 Hz
Hyams and Borisy (1978)	≃25 ± 5 Hz

experimental values. The reason for this is unknown. One possibility is that the *C. reinhardtii* cell is no longer behaving as a R-G-D sphere but is displaying some internal structure.

Summary

The two-speed distribution model with a stationary function and the sine function model when associated with a $P_s(v)$ similar to Fig. 3 result in a model for motility of *C. reinhardtii* which (*a*) matches the HWT of the experimental electric field autocorrelation functions, and (*b*) incorporates a forward-and-reverse motion in the model that is observed cinematographically. The two-speed distribution model with a stationary function also gives an average progressive speed of $\bar{v} = 84$ μm/s, which matches the cinematographical value when the parameters of the model are properly related to the way in which the least-square program fits the data. The model also matches the experimental autocorrelation curve very well.

The result is that the two models, in particular the two-speed distribution model, are quite successful in modeling the light-scattering electric field autocorrelation function information to give results that match the motile characteristics observed in cinematography. The light-scattering analysis required information from cinematography, initially, to help fine-tune the interpretation of the model parameters. Once calibrated, however, the light-scattering system provides a much quicker and more elegant means of determining the mean progressive swimming velocity of a cell culture by sampling of a large number of cells.

We would like to thank Jackie Marsh and Tom Craig for their support and assistance during various stages of the project.

This research is supported by a grant from the Natural Sciences and Engineering Research Council.

Received for publication 7 October 1980 and in revised form 18 March 1981.

REFERENCES

Bean, B., and A. Harris. 1979. Selective inhibition of flagellar activity in *Chlamydomonas* by nickel. *J. Protozool.* 26:235–240.

Craig, T., F. R. Hallett, and B. Nickel. 1979. Quasi-elastic light scattering spectra of swimming spermatozoa. Rotational and translational effects. *Biophys. J.* 28:457–472.

Holz, M., and S.-H. Chen. 1978. Rotational-translational models for interpretation of quasi-elastic light scattering spectra of motile bacteria. *Appl. Opt.* 17:3197–3204.

Hyams, J. S., and G. G. Borisy. 1978. Isolated flagellar apparatus of *Chlamydomonas:* characterization of forward swimming and alteration of waveform and reversal of motion by calcium ions *in vitro*. *J. Cell Sci.* 33:235–253.

Nakamura, S. 1979. A backward swimming mutant of *Chlamydomonas reinhardtii*. *Exp. Cell Res.* 123:441–444.

Nossal, R. 1971. Spectral analysis of laser light scattered from motile microorganism. *Biophys. J.* 4:341–354.

Ringo, David L. 1967. Flagellar motion and fine structure of the flagellar apparatus in *Chlamydomonas*. *J. Cell Biol.* 33:543–571.